



**HAL**  
open science

# Fluid phase equilibria in asymmetric model systems. Part I: CO<sub>2</sub>+ diphenylmethane

Jean-Luc Daridon, J.F. Romero Yanes, F. Montel

► **To cite this version:**

Jean-Luc Daridon, J.F. Romero Yanes, F. Montel. Fluid phase equilibria in asymmetric model systems. Part I: CO<sub>2</sub>+ diphenylmethane. Journal of Supercritical Fluids, 2022, 186, pp.105585. 10.1016/j.supflu.2022.105585 . hal-03693094

**HAL Id: hal-03693094**

**<https://hal.science/hal-03693094v1>**

Submitted on 22 Jul 2024

**HAL** is a multi-disciplinary open access archive for the deposit and dissemination of scientific research documents, whether they are published or not. The documents may come from teaching and research institutions in France or abroad, or from public or private research centers.

L'archive ouverte pluridisciplinaire **HAL**, est destinée au dépôt et à la diffusion de documents scientifiques de niveau recherche, publiés ou non, émanant des établissements d'enseignement et de recherche français ou étrangers, des laboratoires publics ou privés.



Distributed under a Creative Commons Attribution - NonCommercial 4.0 International License

# Fluid phase equilibria in asymmetric model systems.

## Part I: CO<sub>2</sub> + diphenylmethane

J.F. Romero Yanes, F. Montel, J.L. Daridon

Laboratoire des Fluides Complexes et leurs Réservoirs E2S UPPA, CNRS, TOTAL ENERGIES, LFCR,

Université de Pau et des Pays de l'Adour, Pau, 64000, France

\*email: /Telephone:

### Abstract

Asymmetric reservoir fluids with high gas-to-oil ratios and heavy oils could present complex phase behaviors at reservoir or production conditions, as observed in Brazilian Pre-Salt reservoirs. To better understand the phase behaviors of these types of reservoir fluids with high carbon dioxide and methane contents, we initiated a study in our laboratory on the fluid phase equilibria of systems containing supercritical CO<sub>2</sub> and/or methane plus a heavy hydrocarbon. In the initial phase of this program, which forms this article, the choice was made to experimentally determine the phase diagram of the binary system: carbon dioxide + diphenylmethane within the temperature range 293.15 to 378.15 K. In addition, the data were compared with those modeled using a predictive version of the Peng-Robinson equation of state (PPR78).

**Keywords:** Fluid phase equilibria; carbon dioxide; aromatics.

## 24 1. Introduction

25 Due to their impacts on energy production, high pressure reservoirs have been the  
26 topic of numerous studies [1–3]. These reservoirs are characterized by extreme pressures,  
27 often exceeding 50 MPa and temperatures of up to 470 K. Moreover, they can be associated  
28 with fluids that are complex in terms of composition [4]. Some of these reservoir fluids are  
29 classified as asymmetric, with high methane and carbon dioxide content mixed with heavy  
30 hydrocarbons with a significant C<sub>7+</sub> fraction, with molecules that can contain more than 40  
31 carbon atoms [5].

32 The difference in size between the components of asymmetric mixtures can promote  
33 complex types of phase behavior, generally associated with significant deviation from  
34 ideality at high-pressure conditions [6,7]. Even though reservoir fluids are made up of  
35 thousands of different hydrocarbon components, the experiments to study and understand  
36 their phase behavior need to be carried out on a simple model. The model systems most  
37 commonly used for these studies are binary mixtures of methane or carbon dioxide with *n*-  
38 alkanes. Consequently, the phase behavior of these mixtures has been extensively described  
39 in the literature [8–16]. Information concerning the type of phase behavior observed  
40 (according to the classification proposed by van Konynenburg and Scott [17] and the phase  
41 transitions reported as a function of the *n*-alkane carbon number) is summarized in Table 1  
42 for both CH<sub>4</sub> + *n*-alkane and CO<sub>2</sub> + *n*-alkane binary systems.

43 Table 1 shows that as the chain length of the alkanes increases, along with system  
44 asymmetry, a transition from a simple to a more complex phase behavior is observed. More  
45 specifically, the critical behavior of the mixtures shifts from Type I to Type III (according  
46 to van Konynenburg and Scott's classification [17]). In type III behavior, a three-phase

47 liquid – liquid – vapor equilibrium (LLVE) region is obtained at low temperature and  
48 pressures, reaching a critical endpoint near the critical point of the light compound in the  
49 mixture. The phase behavior transitions occur by passing through an intermediate  
50 condition, a type V behavior in the case of methane mixed with *n*-hexane and a type IV  
51 behavior for a methane + *n*-heptane mixture. A Type IV behavior is also observed in the  
52 case of an *n*-tridecane and carbon dioxide system. In the case of heavier alkanes, solid-  
53 phase formation hides liquid-liquid-vapor phase separation, which consequently cannot be  
54 detected in alkanes with a triple point that is much higher than the critical temperature of  
55 the light compound. In these conditions, a solid – liquid – supercritical fluid (SLF) system  
56 is observed, with solid and liquid phases in equilibrium with a supercritical phase with a  
57 high light-component content. This additional fluid phase behaves like a dense phase at  
58 high pressure, and like a dilute phase in low-pressure conditions [10].

59       Among the existing studies concerning the phase behavior of asymmetric light +  
60 heavy hydrocarbon systems, there is a lack of experiments on branched-chain alkanes and  
61 polyaromatic molecules, as can be confirmed by looking at periodic reports concerning  
62 experiments of high-pressure fluid phase equilibria [62–66]. These observations regarding  
63 the lack of data on the fluid phase equilibria of model systems led us to undertake an  
64 experimental and modeling investigation of binary and multi-component synthetic systems,  
65 which could represent complex phase transitions as observed in some reservoir fluids such  
66 as those of Brazil’s Pre-Salt fields. In the initial phase of this program, the subject of this  
67 first article, the choice was made to experimentally determine the phase behavior of the  
68 binary system composed of carbon dioxide and diphenylmethane. Phase transition  
69 measurements were carried out using a synthetic method in the temperature range from  $T =$

70 (293.15 to 378.15) K. Predictive cubic equations of state were also tested to describe the  
71 experimental phase behavior obtained.

72       Some Brazilian Pre-Salt reservoir fluids, characterized by high gas content which can  
73 exceed 55.0 mol% [67–69], presented L-L and L-L-V equilibrium domains at high  
74 temperatures as described in previous studies [69–72]. The L-L phase immiscibility  
75 observed in these fluids under HT-HP conditions (high temperature – high pressure) was  
76 characterized by the formation of a dispersed liquid phase in the continuous oil phase,  
77 which makes difficult to detect phase changes in these types of black oil systems, but above  
78 all, makes it practically impossible to sample and analyze the second liquid phase, thereby  
79 limiting understanding of these phase equilibria. Only by combining experimental and  
80 modeling techniques it was possible to establish that the L-L immiscibility observed in Pre-  
81 Salt oils could be generated by the demixing of heavy hydrocarbon compounds from crude  
82 oils [70] rather than by carbon dioxide separation as usually observed at low temperature in  
83 CO<sub>2</sub> + *n*-alkane systems. Consequently, modeling plays a crucial role in understanding the  
84 complex phase behaviors of these types of reservoir fluids, and their reliability must  
85 therefore be verified using a synthetic system. In view of the requirement to perform proper  
86 modeling, the experimental data were compared using a predictive PPR78 model based on  
87 the Peng Robinson equation of state with the addition of a fully predictive mixing rule,  
88 which is therefore particularly well suited to predicting systems with high molecular weight  
89 components.

90

## 91 2. Materials and Methods

92

### 93 2.1. Chemicals

94 The chemical compounds used to formulate the systems are listed in Table 2, while the  
95 molecular weights, melting temperatures, and normal boiling points of the liquid  
96 compounds are listed in Table 3. All chemicals were used without any further purification.

97

### 98 2.2 Experimental technique

99 A full visual PVT cell was used to study phase behavior and prepare the systems, as  
100 described in a previous paper [33]. In short, the PVT cell is a high-pressure volumetric  
101 piston with a sapphire window at the top that allows total visibility of the cell content.  
102 Operating limits were 100 MPa, 30 cm<sup>3</sup>, and 383.15 K, for pressure, volume, and  
103 temperature, respectively. The PVT cell was adapted using a coupled calibrated pressure  
104 transducer with an uncertainty  $u(p^{gauge})$  of  $\pm 0.02\%$  across its entire range. Temperature  
105 control was made by circulating a heat-carrier fluid through three flow lines directly  
106 managed in the cell body and connected to a thermostatic bath (Ministat 230, Huber with  
107 temperature stability of  $\pm 0.02$  K). Temperature was measured using a Pt-100 directly in  
108 contact with the metal cell body, with an uncertainty  $u(T^{gauge})$  of 0.1 K. Additionally, a  
109 magnetic bar was put inside the cell to continuously stir the sample studied by means of an  
110 external magnetic stirrer system placed beneath the cell.

111 Phase behavior analysis was performed according to the synthetic method at  
112 isoplethic conditions. Isopleth composition was therefore precisely controlled during the

113 synthesis of the mixture before the fluid phase behavior analysis. For that purpose, mixtures  
114 were prepared directly inside the measurement cell by weighing both the liquid and gas.  
115 For this operation, the liquid was first injected into the PVT cell under vacuum, and the  
116 amount of liquid transferred to the cell was determined by using an analytical balance with  
117 uncertainty in measurement equal to 1 mg. The CO<sub>2</sub> was then added under pressure. To  
118 weigh the amount of gas added to the cell, the CO<sub>2</sub> was initially loaded into a large-volume  
119 tank (1 l) and placed on a precision balance with uncertainty in measurement equal to 1 mg.  
120 In order to avoid errors in mass due to the connection between the cell and the tank, a  
121 flexible PEEK tubing with an internal diameter of 1/32" was used to join them. Finally, the  
122 CO<sub>2</sub> was stored at Liquid – Vapor phase equilibrium in the tank to maintain constant  
123 pressure during the injection. Based on this method, the standard uncertainties for the  
124 masses introduced were estimated to be less than 0.005 g for both components, and the  
125 combined standard uncertainty for the feed mole fraction  $z_{CO_2}$  was estimated using the  
126 following relationship:

127

$$128 \quad u_c(z_{CO_2}) = z_{CO_2}(1 - z_{CO_2}) \left( \frac{u^2(m_{CO_2})}{m_{CO_2}^2} + \frac{u^2(m_{arom})}{m_{arom}^2} \right)^{1/2} \quad (1)$$

129

130 After both liquid and gas had been introduced, the prepared mixture was  
131 homogenized at high temperature (378.15 K) and high pressure (well above bubble point  
132 pressure). When single-phase equilibrium was achieved, the phase transition experiments  
133 started by incrementally changing  $p$  conditions. Throughout the change process, vigorous  
134 stirring was activated. The system was then maintained in equilibrium without stirring to  
135 facilitate observation. When a phase appeared, the pressure at which the transition was

136 observed was registered. The standard uncertainty for the phase transition points observed  
 137 was  $u(p^{obs}) = 0.02$  MPa, related to reproducibility of the visual detection of a new formed  
 138 phase. Special care has been taken to visually determine liquid to liquid – liquid phase  
 139 transition (L to LL), mainly related to the high phase dispersity formed at high CO<sub>2</sub> content  
 140 and high pressure. The observation uncertainty was considered alongside those of  
 141 instrument pressure and temperature,  $u(p^{gauge})$ , and  $u(T^{gauge})$ , respectively. Finally,  
 142 expanded uncertainty to determine the phase transition pressure  $U(p^{transition})$  was calculated  
 143 based on the error propagations described in the Guide to the expression of Uncertainty  
 144 Measurement (GUM) of the National Institute of Standards and Technology [73], as  
 145 follows:

146

$$147 \quad U^2(p^{transition}) = u^2(p^{obs}) + u^2(p^{gauge}) + \left[ \left( \frac{\partial p^{obs}}{\partial T} \right) u(T^{gauge}) \right]^2 \quad (2)$$

148

149 Partial derivatives with respect to temperature were obtained by numerical differentiation  
 150 of the data [50]. For each isopleth, constant mass expansion (CME) tests were performed at  
 151 five different temperatures  $T = (293.15, 308.15, 323.15, 338.15, 358.15, \text{ and } 378.15)$  K.

152 For detection of solid phase appearance (L → LS), measurements were taken at isobaric  
 153 conditions and incrementally changing  $T$  up to  $T^{obs}$ . This method was adopted because of  
 154 the steep slope of the L → LS locus. During this procedure, standard uncertainty was  
 155  $u(T^{obs}) = 0.2$  K and expanded uncertainty for LS formation temperature  $U(T^{transition})$  was  
 156 estimated as follows:

157

$$158 \quad U^2(T^{transition}) = u^2(T^{gauge}) + u^2(T^{obs}) + \left[ \left( \frac{\partial T^{obs}}{\partial p} \right) u(p^{gauge}) \right]^2 \quad (3)$$



159

160

### 161 3. Results and discussion

162 The phase behavior of binary systems composed of carbon dioxide and  
163 diphenylmethane was determined based on 11 isoplethic measurements, from 20.13 to  
164 95.03 CO<sub>2</sub> mol%. Fluid phase transitions are presented in Table 4, including L → LV and L  
165 → LL phase transitions as well as LLV phase equilibria. Additionally, solid-fluid phase  
166 transitions L → LS are presented in Table 5. Isoplethic  $pT$  diagrams are presented in Figure  
167 1 and Figure 2 for low and high CO<sub>2</sub> content mixtures, respectively. From these  
168 measurements, it can be concluded that diphenylmethane and CO<sub>2</sub> mixtures present a type  
169 III phase behavior in the van Konynenburg and Scott classification scheme [17].  
170 Accordingly, the critical line linking the pure compounds' critical points is interrupted and  
171 divided into two branches. One of the critical lines goes from the critical point of the  
172 diphenylmethane and increases to higher pressures, while the other critical line connects the  
173 critical point of the carbon dioxide to a triphasic LLV line through an upper critical  
174 endpoint (UCEP).

175 Liquid – liquid immiscibility was first detected in the mixture with 60.18 CO<sub>2</sub> mol %  
176 whose results are depicted in Figure 2. This behavior was not reported before because of  
177 the small dataset available in the literature for diphenylmethane and CO<sub>2</sub> mixtures [74,75].  
178 A comparison between liquid phase compositions obtained by Chung et al. [75] using an  
179 analytical method and our measurements is presented in Figure 3 at  $T=308.15$  K.  
180 Interpolation of our  $p,T$  data must be done for this plot as the isopleth measurements were  
181 not exactly carried out at  $T=308.15$  K. A good graphical agreement is observed between

182 both datasets until 25 MPa but a significant deviation is noted at 30 MPa. At this pressure,  
183 Chung's et al data [75] seems to overestimate CO<sub>2</sub> solubility in liquid phase. This leads to a  
184 significant underestimation of phase transition pressure in the graph with an observed  
185 deviation higher than 10 MPa on the saturation pressure for mixture with 85.0 CO<sub>2</sub> mol %.

186 Additionally, a three-phase LLV equilibria was visually observed at temperatures  
187 below the CO<sub>2</sub> critical point, with the formation of a light vapor phase in equilibrium with  
188 two liquid phases, as depicted in Figure 4. This LLV locus goes from temperatures below  
189 293.15 K until an UCEP corresponding to 306.5 K and 7.70 MPa conditions. For systems  
190 with higher carbon dioxide content, the volume fraction of the light liquid phase increases,  
191 as one can note in Figure 4(c) for the 75.15 CO<sub>2</sub> mol % mixture.

192 Similar behavior has been reported for 1-methylnaphthalene ( $T^m = 242.6$  K) [76], 2-  
193 methylnaphthalene ( $T^m = 306.6$  K) [77], and alkylaromatics mixtures with CO<sub>2</sub> [51,78,79].  
194 The asymmetry and the low melting point of these hydrocarbons lead to the formation of  
195 LL insolubility. This liquid-liquid phase separation is not present in CO<sub>2</sub> + aromatic  
196 systems when the asymmetry is much less significant as in the case of carbon dioxide with  
197 benzene or toluene [80]. The triphasic LLV region is not formed for high condensed  
198 polyaromatics because of their elevated LS transition temperatures [57,81–85]. For these  
199 heavy compounds, the LS locus occludes the LLV equilibria at low temperatures. Because  
200 of the low melting temperature of diphenylmethane (299.0 K) and the decrease in melting  
201 temperature caused by CO<sub>2</sub> addition, no LLS equilibria or LLVS (quadruple  $Q$ -point) can  
202 be detected in the studied temperature and pressure ranges.

203 Isoplethic data were used together with a smoothing function to represent the results  
204 in an isothermal ( $p, z_I$ ) diagram. Polynomial functions were considered to interpolate values  
205 at a given temperature, and results are presented in Table 6 and Figure 5. In addition, these

206 isothermal phase behavior were modeled using the Peng-Robinson equation of state [86]  
207 with its classical mixing rules. The critical temperature  $T_c$  and pressure  $P_c$  of pure  
208 components required to determine  $a_i$  and  $b_i$  parameters of the cubic equation of state were  
209 obtained from the NIST webbook and are presented in Table 7 [87]. There is only one  
210 value of acentric factor for diphenylmethane reported in the literature [88]. However, in this  
211 publication, the critical parameters are much higher than values reported on NIST database,  
212 e.g., the reported critical pressure is 3.28 MPa while NIST average value for  $P_c$  is 2.979  
213 MPa. Considering this divergence in critical properties, the reported value of the acentric  
214 factor for diphenylmethane was not considered. Instead, the acentric factor was calculated  
215 by using the Pitzer's relation, as commonly made for heavy hydrocarbons [89,90]:

216

$$217 \quad \omega = \frac{-\ln(P_c) - 5.92714 + 6.09648 \cdot \theta^{-1} + 1.28862 \cdot \ln(\theta) - 0.169347 \cdot \theta^6}{15.2518 - 15.6875 \cdot \theta^{-1} - 13.4721 \cdot \ln(\theta) + 0.43577 \cdot \theta^6} \quad (4)$$

218

219 where  $\theta = T_b/T_c$ , both temperatures in K, and  $P_c$  in bar.

220

221 Binary interaction parameter  $k_{ij}$  was determined as a function of temperature by  
222 either fitting the experimental data or using PPR78, a predictive version of Peng-Robinson  
223 equation of state based on a group contribution method developed by Jaubert and  
224 collaborators [91–96]. In this fully predictive method, the binary interaction parameter is  
225 given by:

226

$$\begin{aligned}
227 \quad k_{ij}(T) = & \left\{ \left[ -\frac{1}{2} \sum_{k=1}^{N_g} \sum_{l=1}^{N_g} (\alpha_{ik} - \alpha_{jk})(\alpha_{il} - \alpha_{jl}) A_{kl} (298.15/T)^{\left(\frac{B_{kl}}{A_{kl}} - 1\right)} \right] - \right. \\
228 \quad & \left. \left[ \frac{\sqrt{a_i(T)}}{b_i} - \frac{\sqrt{a_j(T)}}{b_j} \right]^2 \right\} \cdot \left( 2 \cdot \frac{\sqrt{a_i(T)a_j(T)}}{b_i b_j} \right)^{-1} \quad (5)
\end{aligned}$$

229

230 where  $N_g$  represents the total number of functional groups considered by the method,  $\alpha_{ik}$  is  
231 the occurrence of group  $k$  in component  $i$  divided by  $N_g$ , and  $A_{kl}$  and  $B_{kl}$  are group  
232 parameters. A total of 21 functional groups for PR78 have been defined [91–96].

233 Results obtained from PR EOS fitting are presented in Figure 5 for all investigated  
234 temperatures. This figure also depicts the phase envelope description obtained by the  
235 predictive PPR78 EOS version. Fitted and predicted binary interaction parameters are listed  
236 in Table 7. The models describe the system phase behavior qualitatively, with significant  
237 deviations in the LL and critical regions. This is expected because of the limited  
238 representation of high asymmetric systems by PR EOS, especially using classical mixing  
239 rules and only the attractive binary interaction parameter [7,97]. However, a good  
240 description of low-pressure LLV is obtained at 293.15 K [98].

241 As one can note in Table 7, there are no significant differences between fitted and  
242 predicted interaction parameters. The PPR78 seems to correctly predict the temperature-  
243 dependent  $k_{ij}$  for diphenylmethane and carbon dioxide, based on the aromatics functional  
244 groups considered by the model [91,99]. Fitted and predicted binary interaction parameters  
245 are in accordance with results reported in the literature for such systems [99]. Optimized  
246  $A_{12}$  and  $B_{12}$  for the PPR78 EOS can be obtained by fitting these parameters to the tuned  
247 temperature-dependent  $k_{ij}$  using Eq. 6, as follows:

248

$$k_{ij}(T) = \left\{ \left[ A_{ij} \cdot (298.15/T)^{\left( \frac{B_{ij}}{A_{ij}} - 1 \right)} \right] - \left[ \frac{\sqrt{a_i(T)}}{b_i} - \frac{\sqrt{a_j(T)}}{b_j} \right]^2 \right\} \cdot \left( 2 \cdot \frac{\sqrt{a_i(T)a_j(T)}}{b_i b_j} \right)^{-1} \quad (6)$$

250

251 In this equation, the molecules  $i$  and  $j$  on the binary mixture are treated as a single group

252 [100,101]. The optimal values obtained were  $A_{12} = 131.81$  MPa and  $B_{12} = 133.74$  MPa.

253 These results can help to improve the group parameters considered in PPR78.

254

255

#### 256 **4. Conclusions**

257 The phase behavior of carbon dioxide and diphenylmethane mixtures was investigated by

258 measuring liquid – vapor, liquid – liquid, liquid – liquid – vapor, and liquid – solid phase

259 equilibria. The isopleth and  $p,x$  phase diagram were constructed from these measurements.

260 Results suggest that this mixture exhibits a type III phase behavior in the van Konynenburg

261 and Scott classification scheme. Liquid – liquid and liquid – liquid – vapor insolubilities

262 were detected at carbon dioxide content above 60.18 mol %. Peng-Robinson equation of

263 state qualitatively describes the experimental phase behavior using temperature-dependent

264 attractive binary interaction parameters, with maximum deviations in the liquid – liquid and

265 critical regions.

266

#### 267 **6. References**

268 [1] E. Flöten, Th.W. de Loos, J. de Swaan Arons, Hyperbaric reservoir fluids: High-

269 pressure phase behavior of asymmetric methane +n-alkane systems, Int. J.

270 Thermophys. 16–16 (1995) 185–194. <https://doi.org/10.1007/BF01438969>.

- 271 [2] F.M. Orr Jr., Carbon Capture, Utilization, and Storage: An Update, *SPE J.* 23 (2018)  
272 2444–2455. <https://doi.org/10.2118/194190-PA>.
- 273 [3] S.Z. Al Ghafri, G.C. Maitland, J.P.M. Trusler, Experimental and modeling study of  
274 the phase behavior of synthetic crude oil+CO<sub>2</sub>, *Fluid Phase Equilibria.* 365 (2014)  
275 20–40. <https://doi.org/10.1016/j.fluid.2013.12.018>.
- 276 [4] E. Flöter, Th.W. de Loos, J. de Swaan Arons, High pressure solid-fluid and vapour-  
277 liquid equilibria in the system (methane + tetracosane), *Fluid Phase Equilibria.* 127  
278 (1997) 129–146. [https://doi.org/10.1016/S0378-3812\(96\)03157-3](https://doi.org/10.1016/S0378-3812(96)03157-3).
- 279 [5] E. Flöter, P. van der Pijl, Th.W. de Loos, J. de Swaan Arons, High-pressure phase  
280 equilibria in the systems methane + phenanthrene and methane + 1-phenyldodecane  
281 up to 400 MPa, *Fluid Phase Equilibria.* 134 (1997) 1–19.  
282 [https://doi.org/10.1016/S0378-3812\(97\)00067-8](https://doi.org/10.1016/S0378-3812(97)00067-8).
- 283 [6] H.J. van der Kooi, E. Flöter, Th.W. de Loos, High-pressure phase equilibria of  
284  $\{(1-x)\text{CH}_4+x\text{CH}_3(\text{CH}_2)_{18}\text{CH}_3\}$ , *J. Chem. Thermodyn.* 27 (1995) 847–861.  
285 <https://doi.org/10.1006/jcht.1995.0089>.
- 286 [7] M. Cismondi Duarte, M.V. Galdo, M.J. Gomez, N.G. Tassin, M. Yanes, High  
287 pressure phase behavior modeling of asymmetric alkane+alkane binary systems with  
288 the RKPR EOS, *Fluid Phase Equilibria.* 362 (2014) 125–135.  
289 <https://doi.org/10.1016/j.fluid.2013.09.039>.
- 290 [8] J. García, L. Lugo, J. Fernández, Phase Equilibria, *PVT Behavior, and Critical*  
291 *Phenomena in Carbon Dioxide + n -Alkane Mixtures Using the Perturbed-Chain*  
292 *Statistical Associating Fluid Theory Approach*, *Ind. Eng. Chem. Res.* 43 (2004) 8345–  
293 8353. <https://doi.org/10.1021/ie049691o>.

- 294 [9] M. Cismondi, S.B. Rodríguez-Reartes, J.M. Milanesio, M.S. Zabaloy, Phase  
295 Equilibria of CO<sub>2</sub> + n-Alkane Binary Systems in Wide Ranges of Conditions:  
296 Development of Predictive Correlations Based on Cubic Mixing Rules, *Ind. Eng.*  
297 *Chem. Res.* 51 (2012) 6232–6250. <https://doi.org/10.1021/ie2018806>.
- 298 [10] M. Campestrini, P. Stringari, Solubilities of solid n-alkanes in methane: Data analysis  
299 and models assessment, *AIChE J.* 64 (2018) 2219–2239.  
300 <https://doi.org/10.1002/aic.16071>.
- 301 [11] H. Quinteros-Lama, F. Llovel, Global phase behaviour in methane plus n-alkanes  
302 binary mixtures, *J. Supercrit. Fluids.* 111 (2016) 151–161.  
303 <https://doi.org/10.1016/j.supflu.2016.01.018>.
- 304 [12] H. Quinteros-Lama, F. Llovel, Global phase behaviour in carbon dioxide plus n-  
305 alkanes binary mixtures, *J. Supercrit. Fluids.* 140 (2018) 147–158.  
306 <https://doi.org/10.1016/j.supflu.2018.06.012>.
- 307 [13] C.E. Schwarz, I. Nieuwoudt, J.H. Knoetze, Phase equilibria of long chain n-alkanes in  
308 supercritical ethane: Review, measurements and prediction, *J. Supercrit. Fluids.* 46  
309 (2008) 226–232. <https://doi.org/10.1016/j.supflu.2008.05.007>.
- 310 [14] I. Polishuk, J. Wisniak, H. Segura, Simultaneous prediction of the critical and sub-  
311 critical phase behavior in mixtures using equations of state II. Carbon dioxide–heavy  
312 n-alkanes, *Chem. Eng. Sci.* 58 (2003) 2529–2550. [https://doi.org/10.1016/S0009-  
313 2509\(03\)00101-5](https://doi.org/10.1016/S0009-2509(03)00101-5).
- 314 [15] N.G. Tassin, S.B. Rodríguez Reartes, M. Cismondi, New Correlations for Prediction  
315 of High-Pressure Phase Equilibria of n-Alkane Mixtures with the RKPR EoS: Back  
316 from the Use of  $l_{ij}$  (Repulsive) Interaction Parameters, *J. Chem. Eng. Data.* 64 (2019)  
317 2093–2109. <https://doi.org/10.1021/acs.jced.8b01050>.

- 318 [16] N.G. Tassin, S.B. Rodríguez Reartes, M.S. Zabaloy, M. Cismondi, Modeling of solid-  
319 fluid equilibria of pure n-alkanes and binary methane + n-alkane systems through  
320 predictive correlations, *J. Supercrit. Fluids*. 166 (2020) 105028.  
321 <https://doi.org/10.1016/j.supflu.2020.105028>.
- 322 [17] P.H. van Konynenburg, R.L. Scott, J.S. Rowlinson, Critical lines and phase equilibria  
323 in binary van der Waals mixtures, *Philos. Trans. R. Soc. Lond. Ser. Math. Phys. Sci.*  
324 298 (1980) 495–540. <https://doi.org/10.1098/rsta.1980.0266>.
- 325 [18] G.P. Kuebler, G. McKinley, Solubility of Solid n-Butane and n-Pentane in Liquid  
326 Methane, in: K.D. Timmerhaus, D.H. Weitzel (Eds.), *Adv. Cryog. Eng.*, Springer US,  
327 Boston, MA, 1975: pp. 509–515. [https://doi.org/10.1007/978-1-4757-0208-8\\_60](https://doi.org/10.1007/978-1-4757-0208-8_60).
- 328 [19] F. Kurata, Solubility of heavier hydrocarbons in liquid methane, Gas Processors  
329 Association, 1975.
- 330 [20] A.J. Davenport, J.S. Rowlinson, The solubility of hydrocarbons in liquid methane,  
331 *Trans. Faraday Soc.* 59 (1963) 78–84. <https://doi.org/10.1039/TF9635900078>.
- 332 [21] J. Shim, J.P. Kohn, Multiphase and Volumetric Equilibria of Methane-n-Hexane  
333 Binary System at Temperatures Between -110° and 150° C., *J. Chem. Eng. Data*. 7  
334 (1962) 3–8. <https://doi.org/10.1021/je60012a002>.
- 335 [22] G.T. Preston, E.W. Funk, J.M. Prausnitz, Solubilities of hydrocarbons and carbon  
336 dioxide in liquid methane and in liquid argon, *J. Phys. Chem.* 75 (1971) 2345–2352.  
337 <https://doi.org/10.1021/j100684a020>.
- 338 [23] Y.-N. Lin, R.J.J. Chen, P.S. Chapple, R. Kobayashi, Vapor-liquid equilibrium of  
339 the methane-n-hexane system at low temperature, *J. Chem. Eng. Data*. 22 (1977) 402–  
340 408. <https://doi.org/10.1021/je60075a007>.



- 341 [24] K.D. Luks, J.D. Hottovy, J.P. Kohn, Three-phase solid-liquid-vapor equilibriums in  
342 the binary hydrocarbon systems methane-n-hexane and methane-benzene, *J. Chem.*  
343 *Eng. Data.* 26 (1981) 402–403. <https://doi.org/10.1021/je00026a016>.
- 344 [25] J.P. Kohn, Heterogeneous phase and volumetric behavior of the methane n-heptane  
345 system at low temperatures, *AIChE J.* 7 (1961) 514–518.  
346 <https://doi.org/10.1002/aic.690070334>.
- 347 [26] R.J.J. Chen, P.S. Chappellear, R. Kobayashi, Dew-point loci for methane-n-hexane and  
348 methane-n-heptane binary systems, *J. Chem. Eng. Data.* 21 (1976) 213–219.  
349 <https://doi.org/10.1021/je60069a025>.
- 350 [27] J.P. Kohn, W.F. Bradish, Multiphase and Volumetric Equilibria of the Methane-n-  
351 Octane System at Temperatures between -110° and 150° C., *J. Chem. Eng. Data.* 9  
352 (1964) 5–8. <https://doi.org/10.1021/je60020a003>.
- 353 [28] J.P. Kohn, K.D. Luks, P.H. Liu, D.L. Tiffin, Three-phase solid-liquid-vapor  
354 equilibriums of the binary hydrocarbon systems methane-n-octane and methane-  
355 cyclohexane, *J. Chem. Eng. Data.* 22 (1977) 419–421.  
356 <https://doi.org/10.1021/je60075a011>.
- 357 [29] L.M. Shipman, J.P. Kohn, Heterogeneous Phase and Volumetric Equilibrium in the  
358 Methane-n-Nonane System., *J. Chem. Eng. Data.* 11 (1966) 176–180.  
359 <https://doi.org/10.1021/je60029a014>.
- 360 [30] J.M. Beaudoin, J.P. Kohn, Multiphase and volumetric equilibria of the methane-n-  
361 decane binary system at temperatures between -36.degree. and 150.degree., *J. Chem.*  
362 *Eng. Data.* 12 (1967) 189–191. <https://doi.org/10.1021/je60033a007>.
- 363 [31] M.P.W.M. Rijkers, V.B. Maduro, C.J. Peters, J. de Swaan Arons, Measurements on  
364 the phase behavior of binary mixtures for modeling the condensation behavior of

365 natural gas: Part II. The system methane + dodecane, *Fluid Phase Equilibria*. 72  
366 (1992) 309–324. [https://doi.org/10.1016/0378-3812\(92\)85033-5](https://doi.org/10.1016/0378-3812(92)85033-5).

367 [32] M. Glaser, C.J. Peters, H.J. Van Der Kool, R.N. Lichtenthaler, Phase equilibria of  
368 (methane + n-hexadecane) and (p, V<sub>m</sub>, T) of n-hexadecane, *J. Chem. Thermodyn.* 17  
369 (1985) 803–815. [https://doi.org/10.1016/0021-9614\(85\)90072-2](https://doi.org/10.1016/0021-9614(85)90072-2).

370 [33] J. Pauly, J. Coutinho, J.-L. Daridon, High pressure phase equilibria in methane+waxy  
371 systems: 1. Methane+heptadecane, *Fluid Phase Equilibria*. 255 (2007) 193–199.  
372 <https://doi.org/10.1016/j.fluid.2007.04.014>.

373 [34] S. Puri, J.P. Kohn, Solid-liquid-vapor equilibrium in the methane-n-eicosane and  
374 ethane-n-eicosane binary systems, *J. Chem. Eng. Data*. 15 (1970) 372–374.  
375 <https://doi.org/10.1021/je60046a024>.

376 [35] J.J.B. Machado, Th.W. de Loos, Liquid–vapour and solid–fluid equilibria for the  
377 system methane + triacontane at high temperature and high pressure, *Fluid Phase*  
378 *Equilibria*. 222–223 (2004) 261–267. <https://doi.org/10.1016/j.fluid.2004.06.003>.

379 [36] F.H. Poettmann, D.L. Katz, Phase Behavior of Binary Carbon Dioxide-Paraffin  
380 Systems, *Ind. Eng. Chem.* 37 (1945) 847–853. <https://doi.org/10.1021/ie50429a017>.

381 [37] T.S. Brown, A.J. Kidnay, E.D. Sloan, Vapor—liquid equilibria in the carbon dioxide-  
382 ethane system, *Fluid Phase Equilibria*. 40 (1988) 169–184.  
383 [https://doi.org/10.1016/0378-3812\(88\)80028-1](https://doi.org/10.1016/0378-3812(88)80028-1).

384 [38] Y.-H. Li, K.H. Dillard, R.L. Robinson, Vapor-liquid phase equilibrium for carbon  
385 dioxide-n-hexane at 40, 80, and 120 .degree.C, *J. Chem. Eng. Data*. 26 (1981) 53–55.  
386 <https://doi.org/10.1021/je00023a018>.

- 387 [39] U.K. Im, Fred. Kurata, Heterogeneous phase behavior of carbon dioxide in n-hexane  
388 and n-heptane at low temperatures, *J. Chem. Eng. Data.* 16 (1971) 412–415.  
389 <https://doi.org/10.1021/je60051a011>.
- 390 [40] H. Kalra, H. Kubota, D.B. Robinson, H.-J. Ng, Equilibrium phase properties of the  
391 carbon dioxide-n-heptane system, *J. Chem. Eng. Data.* 23 (1978) 317–321.  
392 <https://doi.org/10.1021/je60079a016>.
- 393 [41] G. Schneider, Z. Alwani, W. Heim, E. Horvath, E.U. Franck, Phasengleichgewichte  
394 und kritische Erscheinungen in binären Mischsystemen bis 1500 bar, CO<sub>2</sub> mit n-  
395 Octan, n-Undecan, n-Tridecan und n-Hexadecan, *Chem. Ing. Tech. - CIT.* 39 (1967)  
396 649–656. <https://doi.org/10.1002/cite.330391103>.
- 397 [42] J.D. Hottovy, J.P. Kohn, K.D. Luks, Partial miscibility behavior of the ternary systems  
398 methane-propane-n-octane, methane-n-butane-n-octane, and methane-carbon dioxide-  
399 n-octane, *J. Chem. Eng. Data.* 27 (1982) 298–302.  
400 <https://doi.org/10.1021/je00029a020>.
- 401 [43] D.W. Jennings, R.C. Schucker, Comparison of High-Pressure Vapor–Liquid  
402 Equilibria of Mixtures of CO<sub>2</sub> or Propane with Nonane and C<sub>9</sub> Alkylbenzenes, *J.*  
403 *Chem. Eng. Data.* 41 (1996) 831–838. <https://doi.org/10.1021/je960033n>.
- 404 [44] H.M. Sebastian, J.J. Simnick, H.-M. Lin, K.-C. Chao, Vapor-liquid equilibrium in  
405 binary mixtures of carbon dioxide + n-decane and carbon dioxide + n-hexadecane, *J.*  
406 *Chem. Eng. Data.* 25 (1980) 138–140. <https://doi.org/10.1021/je60085a012>.
- 407 [45] A.A. Kukarni, B.Y. Zarah, K.D. Luks, J.P. Kohn, Phase-equilibriums behavior of  
408 system carbon dioxide-n-decane at low temperatures, *J. Chem. Eng. Data.* 19 (1974)  
409 92–94. <https://doi.org/10.1021/je60060a005>.

- 410 [46] J.D. Hottovy, K.D. Luks, J.P. Kohn, Three-phase liquid-liquid-vapor equilibriums  
411 behavior of certain binary carbon dioxide-n-paraffin systems, *J. Chem. Eng. Data.* 26  
412 (1981) 256–258. <https://doi.org/10.1021/je00025a009>.
- 413 [47] R. Enick, G.D. Holder, B.I. Morsi, Critical and three phase behavior in the carbon  
414 dioxide/tridecane system, *Fluid Phase Equilibria.* 22 (1985) 209–224.  
415 [https://doi.org/10.1016/0378-3812\(85\)85020-2](https://doi.org/10.1016/0378-3812(85)85020-2).
- 416 [48] D.J. Fall, K.D. Luks, Liquid-liquid-vapor phase equilibria of the binary system carbon  
417 dioxide + n-tridecane, *J. Chem. Eng. Data.* 30 (1985) 276–279.  
418 <https://doi.org/10.1021/je00041a012>.
- 419 [49] H. Kim, H.-M. Lin, K.-C. Chao, Vapor-liquid equilibrium in binary mixtures of  
420 carbon dioxide plus n-propylcyclohexane and carbon dioxide plus n-octadecane,  
421 *AIChE Symposium Series*, 81 (1985), 101.
- 422 [50] J.-L. Daridon, F. Montel, D.V. Nichita, J. Pauly, Fluid-fluid and fluid-solid phase  
423 equilibria in carbon dioxide + waxy systems 1. CO<sub>2</sub> + n-C<sub>17</sub>, *Fluid Phase Equilibria.*  
424 538 (2021) 113023. <https://doi.org/10.1016/j.fluid.2021.113023>.
- 425 [51] D.J. Fall, K.D. Luks, Liquid-liquid-vapor equilibria of the binary mixtures carbon  
426 dioxide + n-pentadecylbenzene and carbon dioxide + n-nonylbenzene, *Fluid Phase*  
427 *Equilibria.* 23 (1985) 259–267. [https://doi.org/10.1016/0378-3812\(85\)90010-X](https://doi.org/10.1016/0378-3812(85)90010-X).
- 428 [52] D.J. Fall, J.L. Fall, K.D. Luks, Liquid-liquid-vapor immiscibility limits in carbon  
429 dioxide + n-paraffin mixtures, *J. Chem. Eng. Data.* 30 (1985) 82–88.  
430 <https://doi.org/10.1021/je00039a028>.
- 431 [53] N.C. Huie, K.D. Luks, J.P. Kohn, Phase-equilibriums behavior of systems carbon  
432 dioxide-n-eicosane and carbon dioxide-n-decane-n-eicosane, *J. Chem. Eng. Data.* 18  
433 (1973) 311–313. <https://doi.org/10.1021/je60058a008>.

- 434 [54] D.J. Fall, K.D. Luks, Phase equilibria behavior of the systems carbon dioxide + n-  
435 dotriacontane and carbon dioxide + n-docosane, *J. Chem. Eng. Data.* 29 (1984) 413–  
436 417. <https://doi.org/10.1021/je00038a013>.
- 437 [55] A. Kordikowski, G.M. Schneider, Fluid phase equilibria of binary and ternary  
438 mixtures of supercritical carbon dioxide with low-volatility organic substances up to  
439 100 MPa and 393 K: c, *Fluid Phase Equilibria.* 90 (1993) 149–162.  
440 [https://doi.org/10.1016/0378-3812\(93\)85010-J](https://doi.org/10.1016/0378-3812(93)85010-J).
- 441 [56] V.S. Smith, P.O. Campbell, V. Vandana, A.S. Teja, Solubilities of long-chain  
442 hydrocarbons in carbon dioxide, *Int. J. Thermophys.* 17 (1996) 23–33.  
443 <https://doi.org/10.1007/BF01448206>.
- 444 [57] M.A. McHugh, T.J. Yogan, Three-phase solid-liquid-gas equilibria for three carbon  
445 dioxide-hydrocarbon solid systems, two ethane-hydrocarbon solid systems, and two  
446 ethylene-hydrocarbon solid systems, *J. Chem. Eng. Data.* 29 (1984) 112–115.  
447 <https://doi.org/10.1021/je00036a001>.
- 448 [58] E. Reverchon, P. Russo, A. Stassi, Solubilities of solid octacosane and triacontane in  
449 supercritical carbon dioxide, *J. Chem. Eng. Data.* 38 (1993) 458–460.  
450 <https://doi.org/10.1021/je00011a034>.
- 451 [59] M. Spee, G.M. Schneider, Fluid phase equilibrium studies on binary and ternary  
452 mixtures of carbon dioxide with hexadecane, 1-dodecanol, 1,8-octanediol and  
453 dotriacontane at 393.2 K and at pressures up to 100 MPa, *Fluid Phase Equilibria.* 65  
454 (1991) 263–274. [https://doi.org/10.1016/0378-3812\(91\)87029-9](https://doi.org/10.1016/0378-3812(91)87029-9).
- 455 [60] F.N. Tsai, J.S. Yau, Solubility of carbon dioxide in n-tetracosane and in n-  
456 dotriacontane, *J. Chem. Eng. Data.* 35 (1990) 43–45.  
457 <https://doi.org/10.1021/je00059a014>.

- 458 [61] K.A.M. Gasem, R.L. Robinson, Solubilities of carbon dioxide in heavy normal  
459 paraffins (C<sub>20</sub>-C<sub>44</sub>) at pressures to 9.6 MPa and temperatures from 323 to 423 K, J.  
460 Chem. Eng. Data. 30 (1985) 53–56. <https://doi.org/10.1021/je00039a018>.
- 461 [62] R.E. Fornari, P. Alessi, I. Kikic, High pressure fluid phase equilibria: experimental  
462 methods and systems investigated (1978–1987), Fluid Phase Equilibria. 57 (1990) 1–  
463 33. [https://doi.org/10.1016/0378-3812\(90\)80010-9](https://doi.org/10.1016/0378-3812(90)80010-9).
- 464 [63] R. Dohrn, G. Brunner, High-pressure fluid-phase equilibria: Experimental methods  
465 and systems investigated (1988–1993), Fluid Phase Equilibria. 106 (1995) 213–282.  
466 [https://doi.org/10.1016/0378-3812\(95\)02703-H](https://doi.org/10.1016/0378-3812(95)02703-H).
- 467 [64] M. Christov, R. Dohrn, High-pressure fluid phase equilibria: Experimental methods  
468 and systems investigated (1994–1999), Fluid Phase Equilibria. 202 (2002) 153–218.  
469 [https://doi.org/10.1016/S0378-3812\(02\)00096-1](https://doi.org/10.1016/S0378-3812(02)00096-1).
- 470 [65] R. Dohrn, S. Peper, J.M.S. Fonseca, High-pressure fluid-phase equilibria:  
471 Experimental methods and systems investigated (2000–2004), Fluid Phase Equilibria.  
472 288 (2010) 1–54. <https://doi.org/10.1016/j.fluid.2009.08.008>.
- 473 [66] J.M.S. Fonseca, R. Dohrn, S. Peper, High-pressure fluid-phase equilibria:  
474 Experimental methods and systems investigated (2005–2008), Fluid Phase Equilibria.  
475 300 (2011) 1–69. <https://doi.org/10.1016/j.fluid.2010.09.017>.
- 476 [67] R.L.C. Beltrao, C.L. Sombra, A.C.V.M. Lage, J.R.F. Netto, C.C.D. Henriques, SS:  
477 Pre-salt Santos basin - Challenges and New Technologies for the Development of the  
478 Pre-salt Cluster, Santos Basin, Brazil, in: Offshore Technology Conference, 2009.  
479 <https://doi.org/10.4043/19880-MS>.
- 480 [68] C.T. da Costa Fraga, A.C. Capeleiro Pinto, C.C.M. Branco, J.O. de Sant'Anna  
481 Pizarro, C.A. da Silva Paulo, Brazilian Pre-Salt: An Impressive Journey from Plans

482 and Challenges to Concrete Results, in: Offshore Technology Conference, 2015.  
483 <https://doi.org/10.4043/25710-MS>.

484 [69] J.-L. Daridon, C.-W. Lin, H. Carrier, J. Pauly, F.P. Fleming, Combined Investigations  
485 of Fluid Phase Equilibria and Fluid–Solid Phase Equilibria in Complex CO<sub>2</sub>–Crude  
486 Oil Systems under High Pressure, *J. Chem. Eng. Data.* 65 (2020) 3357–3372.  
487 <https://doi.org/10.1021/acs.jced.0c00144>.

488 [70] J.F. Romero Yanes, H.B. de Sant’Ana, F.X. Feitosa, M. Pujol, J. Collell, J. Pauly, F.P.  
489 Fleming, F. Montel, J.-L. Daridon, Study of Liquid–Liquid and Liquid–Liquid–Vapor  
490 Equilibria for Crude Oil Mixtures with Carbon Dioxide and Methane Using Short-  
491 Wave Infrared Imaging: Experimental and Thermodynamic Modeling, *Energy Fuels.*  
492 34 (2020) 14109–14123. <https://doi.org/10.1021/acs.energyfuels.0c03064>.

493 [71] J.F. Romero Yanes, A.F.B. Ferreira, P.Y. Gomes de Medeiros, G.S. Bassani, F.P.  
494 Fleming, F.X. Feitosa, H.B. de Sant’Ana, Phase Behavior for Crude Oil and Methane  
495 Mixtures: Crude Oil Property Comparison, *Energy Fuels.* (2019).  
496 <https://doi.org/10.1021/acs.energyfuels.9b03560>.

497 [72] J.F. Romero Yanes, F.X. Feitosa, F.P. Fleming, H.B. de Sant’Ana, Measurement of  
498 Fluid Phase Equilibria for High Gas Ratio Mixtures of Carbon Dioxide, Methane, and  
499 Brazilian Presalt Crude Oil, *J. Chem. Eng. Data.* 66 (2021) 1356–1366.  
500 <https://doi.org/10.1021/acs.jced.0c00988>.

501 [73] ISO/IEC GUIDE 98-3:2008(E) Guide to the expression of uncertainty in measurement  
502 (GUM:1995). First Edition. 2008, n.d.

503 [74] H.M. Sebastian, G.D. Nageshwar, H.-M. Lin, K.-C. Chao, Vapor-liquid equilibrium in  
504 binary mixtures of carbon dioxide + diphenylmethane and carbon dioxide + 1-

505 methyl-naphthalene, *J. Chem. Eng. Data.* 25 (1980) 145–147.  
506 <https://doi.org/10.1021/je60085a016>.

507 [75] S.T. Chung, K.S. Shing, Multiphase behavior of binary and ternary systems of heavy  
508 aromatic hydrocarbons with supercritical carbon dioxide. Part I. Experimental results,  
509 *Fluid Phase Equilibria.* 81 (1992) 321–341. [https://doi.org/10.1016/0378-](https://doi.org/10.1016/0378-3812(92)85160-A)  
510 [3812\(92\)85160-A](https://doi.org/10.1016/0378-3812(92)85160-A).

511 [76] L.E. Gutiérrez M, K.D. Luks, Three-Phase Liquid–Liquid–Vapor Equilibria of the  
512 Binary Mixture Carbon Dioxide + 1-Methylnaphthalene, *J. Chem. Eng. Data.* 46  
513 (2001) 679–682. <https://doi.org/10.1021/je000322i>.

514 [77] A.A. Kulkarni, K.D. Luks, J.P. Kohn, Phase-equilibriums behavior of systems carbon  
515 dioxide-2-methylnaphthalene and carbon dioxide-n-decane-2-methylnaphthalene, *J.*  
516 *Chem. Eng. Data.* 19 (1974) 349–354. <https://doi.org/10.1021/je60063a025>.

517 [78] D.L. Tiffin, A.L. De Vera, K.D. Luks, J.P. Kohn, Phase-equilibriums behavior of the  
518 binary systems carbon dioxide-n-butylbenzene and carbon dioxide-trans-decalin, *J.*  
519 *Chem. Eng. Data.* 23 (1978) 45–47. <https://doi.org/10.1021/je60076a012>.

520 [79] R.M. Lansangan, A. Jangkamolkulchai, K.D. Luks, Binary vapor liquid equilibria  
521 behavior in the vicinity of liquid liquid vapor loci, *Fluid Phase Equilibria.* 36 (1987)  
522 49–66. [https://doi.org/10.1016/0378-3812\(87\)85013-6](https://doi.org/10.1016/0378-3812(87)85013-6).

523 [80] C.-H. Kim, P. Vimalchand, M.D. Donohue, Vapor-liquid equilibria for binary  
524 mixtures of carbon dioxide with benzene, toluene and p-xylene, *Fluid Phase*  
525 *Equilibria.* 31 (1986) 299–311. [https://doi.org/10.1016/0378-3812\(86\)87014-5](https://doi.org/10.1016/0378-3812(86)87014-5).

526 [81] A. Diefenbacher, M. Türk, Phase equilibria of organic solid solutes and supercritical  
527 fluids with respect to the RESS process, *J. Supercrit. Fluids.* 22 (2002) 175–184.  
528 [https://doi.org/10.1016/S0896-8446\(01\)00123-1](https://doi.org/10.1016/S0896-8446(01)00123-1).



- 529 [82] R.M. Lemert, K.P. Johnston, Solid-liquid-gas equilibria in multicomponent  
530 supercritical fluid systems, *Fluid Phase Equilibria*. 45 (1989) 265–286.  
531 [https://doi.org/10.1016/0378-3812\(89\)80262-6](https://doi.org/10.1016/0378-3812(89)80262-6).
- 532 [83] K. Fukné-Kokot, A. König, Ž. Knez, M. Škerget, Comparison of different methods for  
533 determination of the S–L–G equilibrium curve of a solid component in the presence of  
534 a compressed gas, *Fluid Phase Equilibria*. 173 (2000) 297–310.  
535 [https://doi.org/10.1016/S0378-3812\(00\)00437-4](https://doi.org/10.1016/S0378-3812(00)00437-4).
- 536 [84] P.L. Cheong, D. Zhang, K. Ohgaki, B.C.-Y. Lu, High pressure phase equilibria for  
537 binary systems involving a solid phase, *Fluid Phase Equilibria*. 29 (1986) 555–562.  
538 [https://doi.org/10.1016/0378-3812\(86\)85054-3](https://doi.org/10.1016/0378-3812(86)85054-3).
- 539 [85] E. Bertakis, I. Lemonis, S. Katsoufis, E. Voutsas, R. Dohrn, K. Magoulas, D. Tassios,  
540 Measurement and thermodynamic modeling of solid–liquid–gas equilibrium of some  
541 organic compounds in the presence of CO<sub>2</sub>, *J. Supercrit. Fluids*. 41 (2007) 238–245.  
542 <https://doi.org/10.1016/j.supflu.2006.10.003>.
- 543 [86] D.-Y. Peng, D.B. Robinson, A New Two-Constant Equation of State, *Ind. Eng. Chem.*  
544 *Fundam.* 15 (1976) 59–64. <https://doi.org/10.1021/i160057a011>.
- 545 [87] P.J. Linstrom, W.G. Mallard, NIST Chemistry WebBook, NIST Standard Reference  
546 Database Number 69, National Institute of Standards and Technology, Gaithersburg  
547 MD, n.d.
- 548 [88] R.D. Chirico, W.V. Steele, Thermodynamic Properties of Diphenylmethane, *J. Chem.*  
549 *Eng. Data*. 50 (2005) 1052–1059. <https://doi.org/10.1021/je050034s>.
- 550 [89] V.A. Bychinsky, A.A. Tupitsyn, K.V. Chudnenko, A.V. Mukhetdinova, Methods for  
551 Calculating the Critical Constants of Hydrocarbons (Using the n-Alkane Series as an

552 Example), *J. Chem. Eng. Data.* 58 (2013) 3102–3109.  
553 <https://doi.org/10.1021/je400547n>.

554 [90] B.I. Lee, M.G. Kesler, A generalized thermodynamic correlation based on three-  
555 parameter corresponding states, *AIChE J.* 21 (1975) 510–527.  
556 <https://doi.org/10.1002/aic.690210313>.

557 [91] J.-N. Jaubert, S. Vitu, F. Mutelet, J.-P. Corriou, Extension of the PPR78 model  
558 (predictive 1978, Peng–Robinson EOS with temperature dependent kij calculated  
559 through a group contribution method) to systems containing aromatic compounds,  
560 *Fluid Phase Equilibria.* 237 (2005) 193–211.  
561 <https://doi.org/10.1016/j.fluid.2005.09.003>.

562 [92] J.-N. Jaubert, J. Qian, R. Privat, C.F. Leibovici, Reliability of the correlation allowing  
563 the kij to switch from an alpha function to another one in hydrogen-containing  
564 systems, *Fluid Phase Equilibria.* 338 (2013) 23–29.  
565 <https://doi.org/10.1016/j.fluid.2012.10.016>.

566 [93] J.-N. Jaubert, F. Mutelet, VLE predictions with the Peng–Robinson equation of state  
567 and temperature dependent kij calculated through a group contribution method, *Fluid*  
568 *Phase Equilibria.* 224 (2004) 285–304. <https://doi.org/10.1016/j.fluid.2004.06.059>.

569 [94] J.-N. Jaubert, R. Privat, Relationship between the binary interaction parameters (kij)  
570 of the Peng–Robinson and those of the Soave–Redlich–Kwong equations of state:  
571 Application to the definition of the PR2SRK model, *Fluid Phase Equilibria.* 295  
572 (2010) 26–37. <https://doi.org/10.1016/j.fluid.2010.03.037>.

573 [95] S. Vitu, J.-N. Jaubert, J. Pauly, J.-L. Daridon, D. Barth, Bubble and Dew Points of  
574 Carbon Dioxide + a Five-Component Synthetic Mixture: Experimental Data and

575 Modeling with the PPR78 Model, *J. Chem. Eng. Data.* 52 (2007) 1851–1855.  
576 <https://doi.org/10.1021/je7001978>.

577 [96] S. Vitu, J.-N. Jaubert, F. Mutelet, Extension of the PPR78 model (Predictive 1978,  
578 Peng–Robinson EOS with temperature dependent kij calculated through a group  
579 contribution method) to systems containing naphthenic compounds, *Fluid Phase*  
580 *Equilibria.* 243 (2006) 9–28. <https://doi.org/10.1016/j.fluid.2006.02.004>.

581 [97] M. Cismondi, J.M. Mollerup, M.S. Zabaloy, Equation of state modeling of the phase  
582 equilibria of asymmetric CO<sub>2</sub>+n-alkane binary systems using mixing rules cubic with  
583 respect to mole fraction, *J. Supercrit. Fluids.* 55 (2010) 671–681.  
584 <https://doi.org/10.1016/j.supflu.2010.10.007>.

585 [98] S.B. Rodriguez-Reartes, M. Cismondi, E. Franceschi, M.L. Corazza, J.V. Oliveira,  
586 M.S. Zabaloy, High-pressure phase equilibria of systems carbon dioxide+n-eicosane  
587 and propane+n-eicosane, *J. Supercrit. Fluids.* 50 (2009) 193–202.  
588 <https://doi.org/10.1016/j.supflu.2009.06.017>.

589 [99] S. Vitu, R. Privat, J.-N. Jaubert, F. Mutelet, Predicting the phase equilibria of  
590 CO<sub>2</sub>+hydrocarbon systems with the PPR78 model (PR EOS and kij calculated  
591 through a group contribution method), *J. Supercrit. Fluids.* 45 (2008) 1–26.  
592 <https://doi.org/10.1016/j.supflu.2007.11.015>.

593 [100] S. Zid, J.-P. Bazile, J.-L. Daridon, A. Piña-Martinez, J.-N. Jaubert, S. Vitu, Fluid  
594 phase equilibria for the CO<sub>2</sub> + 2,3-dimethylbutane binary system from 291.9 K to  
595 373.1 K, *J. Supercrit. Fluids.* 179 (2022) 105387.  
596 <https://doi.org/10.1016/j.supflu.2021.105387>.

597 [101] S. Zid, J.-P. Bazile, J.-L. Daridon, J.-N. Jaubert, J.-L. Havet, M. Debaq, S. Vitu,  
598 High-Pressure Phase Equilibria Measurements of the Carbon Dioxide + Cycloheptane  
599 Binary System, J. Chem. Eng. Data. (2021). <https://doi.org/10.1021/acs.jced.1c00848>.  
600  
601

602 Table 1. Fluid phase transitions reported in literature for mixtures of *n*-paraffins and  
 603 methane or carbon dioxide.

System	Type of equilibria	Type of Phase diagram	References
$\text{CH}_4 + \text{n-C}_{(i)}\text{H}_{(2i+2)} / i \in [2 - 5]$	LVE	I	[18–20]
$\text{CH}_4 + \text{n-C}_6\text{H}_{14}$	LVE/ LLE/LLVE	V	[21–24]
$\text{CH}_4 + \text{n-C}_7\text{H}_{16}$	LVE/ LLE/LLVE	IV	[25,26]
$\text{CH}_4 + \text{n-C}_{(i)}\text{H}_{(2i+2)} / i \geq 8$	LFE/SLFE	III	[27–35]
$\text{CO}_2 + \text{n-C}_{(i)}\text{H}_{(2i+2)} / i \in [2 - 6]$	LVE	I	[36–38]
$\text{CO}_2 + \text{n-C}_{(i)}\text{H}_{(2i+2)} / i \in [7 - 11]$	LVE/LLE/LLVE	II	[39–45]
$\text{CO}_2 + \text{n-C}_{12}\text{H}_{26}$	LVE/ LLE/LLVE	- <sup>a</sup>	[46]
$\text{CO}_2 + \text{n-C}_{13}\text{H}_{28}$	LVE/ LLE/LLVE	IV	[47,48]
$\text{CO}_2 + \text{n-C}_{(i)}\text{H}_{(2i+2)} / i \in [14 - 21]$	LVE/ LLE/LLVE	III	[41,46,49–53]
$\text{CO}_2 + \text{n-C}_{(i)}\text{H}_{(2i+2)} / i \geq 22$	LFE/SLFE	III	[54–61]

604 <sup>a</sup> Phase behavior not defined [8]

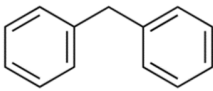
605

606

607

608

609 Table 2. CAS registry number, molecular structure, purity, and suppliers of the chemicals.

Compound	CAS Reg. No.	molecular structure	purity, %	supplier
carbon dioxide	124-38-9	CO <sub>2</sub>	99.995 <sup>a</sup>	Linde
diphenylmethane	101-81-5		99.9 <sup>b</sup>	Sigma-Aldrich

610 <sup>a</sup> molar composition. <sup>b</sup> mass composition reported by the supplier (certificated by gas

611 chromatography)

612

613

614 Table 3. Chemicals molecular weight, melting temperature ( $T^m$ ), and normal boiling  
615 temperature ( $T^b$ ).

Compound	$MW$	$T^m / K$	$T^b / K$
diphenylmethane	168.23	299.0	537.5

616

617 Table 4. Pressure of phase transition  $p$  at a given temperature  $T$  in different mixtures of  
618 global CO<sub>2</sub> composition  $z_{CO_2} \pm U(z_{CO_2})$  in mol % with its expanded ( $k = 2$ ) uncertainty  $U(p)$ .

$T \pm$ 0.1 / K	$p /$ MPa	$U(p) /$ MPa	transition type	$T \pm$ 0.1 / K	$p /$ MPa	$U(p) /$ MPa	transition type	$T \pm$ 0.1 / K	$p /$ MPa	$U(p) /$ MPa	transition type
$z_{CO_2} = 20.13 \pm 0.09$ mol %				$z_{CO_2} = 30.21 \pm 0.09$ mol %				$z_{CO_2} = 40.20 \pm 0.08$ mol %			
293.3	2.27	0.02	L→LV	292.8	3.35	0.02	L→LV	292.8	4.43	0.02	L→LV
307.5	2.75	0.02	L→LV	308.3	4.21	0.03	L→LV	308.0	5.70	0.03	L→LV
323.4	3.32	0.03	L→LV	322.9	5.08	0.03	L→LV	322.9	7.07	0.03	L→LV
338.1	3.91	0.03	L→LV	337.5	6.04	0.03	L→LV	337.5	8.45	0.03	L→LV
357.9	4.66	0.03	L→LV	357.1	7.30	0.03	L→LV	357.5	10.28	0.04	L→LV
377.2	5.29	0.03	L→LV	377.3	8.45	0.04	L→LV	377.2	11.99	0.04	L→LV
$z_{CO_2} = 50.18 \pm 0.07$ mol %				$z_{CO_2} = 60.18 \pm 0.03$ mol %				$z_{CO_2} = 70.17 \pm 0.03$ mol %			
292.9	5.30	0.02	L→LV	293.2	5.70	0.03	LL→LLV	292.9	5.62	0.03	LL→LLV
308.0	7.12	0.04	L→LV	298.0	6.51	0.02	LL→LLV	297.4	6.37	0.02	LL→LLV
323.1	9.20	0.04	L→LV	303.2	7.08	0.03	LL→LLV	302.9	7.00	0.02	LL→LLV
337.8	11.32	0.04	L→LV	306.5	7.70	0.03	UCEP	292.7	52.4	0.3	LL→LLV
357.6	13.90	0.04	L→LV	293.2	15.4	0.1	L→LL	297.4	39.9	0.2	L→LL
377.5	16.27	0.04	L→LV	298.1	13.61	0.09	L→LL	302.9	32.56	0.09	L→LL
				303.0	12.73	0.07	L→LL	308.0	28.91	0.06	L→LL
				306.5	12.63	0.02	L→LL	312.9	27.11	0.05	L→LL
				307.0	12.63	0.02	L→LL	322.9	24.64	0.03	L→LV
				308.0	12.58	0.06	L→LL	337.6	24.46	0.03	L→LV
				313.4	12.88	0.05	L→LL	357.3	26.02	0.03	L→LV
				323.4	13.97	0.04	L→LV	376.7	28.00	0.03	L→LV
				338.0	16.13	0.04	L→LV				
				358.0	19.18	0.03	L→LV				
				376.9	21.56	0.03	L→LV				
$z_{CO_2} = 75.15 \pm 0.02$ mol %				$z_{CO_2} = 80.13 \pm 0.02$ mol %				$z_{CO_2} = 85.10 \pm 0.01$ mol %			
292.8	5.57	0.03	LL→LLV	293.1	5.61	0.03	LL→LLV	293.1	5.63	0.03	LL→LLV
298.0	6.43	0.02	LL→LLV	298.2	6.45	0.02	LL→LLV	298.0	6.40	0.02	LL→LLV



303.0	7.00	0.02	LL→LLV	303.2	7.04	0.02	LL→LLV	303.2	7.01	0.02	LL→LLV
297.4	54.40	0.21	L→LL	303.3	57.77	0.16	L→LL	303.2	70.9	0.2	L→LL
303.1	42.79	0.14	L→LL	307.9	50.88	0.15	L→LL	308.2	61.0	0.2	L→LL
308.1	37.04	0.10	L→LL	312.9	43.49	0.12	L→LL	313.2	52.5	0.2	L→LL
313.4	33.20	0.06	L→LL	317.9	37.88	0.08	L→LL	317.6	44.6	0.1	L→LL
322.7	29.86	0.03	L→LV	322.9	33.90	0.04	L→LL	322.8	37.68	0.04	L→LL
338.1	28.40	0.02	L→LV	327.8	32.20	0.02	L→LV	328.2	35.69	0.02	L→LV
357.6	29.11	0.02	L→LV	338.0	31.06	0.02	L→LV	338.0	34.63	0.02	L→LV
377.7	30.53	0.02	L→LV	357.5	30.96	0.02	L→LV	357.5	33.33	0.02	L→LV
				377.0	32.40	0.02	L→LV	377.2	33.39	0.02	L→LV

$z_{CO_2} = 90.07 \pm 0.01 \text{ mol } \%$

$z_{CO_2} = 95.03 \pm 0.01 \text{ mol } \%$

292.8	5.62	0.03	LL→LLV	293.0	5.53	0.03	LL→LLV
297.9	6.39	0.02	LL→LLV	298.0	6.35	0.02	LL→LLV
303.3	7.04	0.02	LL→LLV	303.2	6.96	0.02	LL→LLV
				292.8	17.87	0.13	V→LV
297.7	69.43	0.30	L→LL	297.7	18.12	0.13	V→LV
303.2	54.48	0.27	F→FF	303.2	18.42	0.09	V→LV
308.2	41.99	0.08	F→FF	307.7	18.62	0.06	V→LV
322.7	33.70	0.04	F→FF	322.8	20.06	0.04	V→LV
338.0	32.60	0.03	V→LV	338.0	22.33	0.04	V→LV
357.5	31.15	0.03	V→LV	357.8	25.09	0.03	V→LV
377.2	32.70	0.03	V→LV	377.2	27.66	0.03	V→LV

619

620

621

622

623

624

625

626 Table 5. Fluid-solid transition temperature at a given pressure  $p$  with its expanded ( $k = 2$ )  
 627 uncertainty  $U(T) = 0.42$  K

$p \pm 0.1$ / MPa	$T$ / K	$p \pm 0.1$ / MPa	$T$ / K
$z_{CO_2} = 20.13 \pm 0.09$ mol %		$z_{CO_2} = 30.21 \pm 0.09$ mol %	
12.0	293.71	23.2	292.71
20.7	296.01	42.9	298.00
29.9	298.00	35.9	296.01
34.9	299.80		
$z_{CO_2} = 40.20 \pm 0.08$ mol %		$z_{CO_2} = 50.18 \pm 0.07$ mol %	
38.6	293.01	52.3	293.01
48.4	295.51		

628

629

630

631 Table 6. Interpolated data of transition pressure  $p$  at isothermal conditions from data  
 632 reported in Table 4.

$T/K$	$p/\text{MPa}$	transition type	$T/K$	$p/\text{MPa}$	transition type	$T/K$	$p/\text{MPa}$	transition type
$z_{\text{CO}_2} = 20.13 \pm 0.09 \text{ mol } \%$			$z_{\text{CO}_2} = 30.21 \pm 0.09 \text{ mol } \%$			$z_{\text{CO}_2} = 40.20 \pm 0.08 \text{ mol } \%$		
293.15	2.25	L→LV	293.15	3.32	L→LV	293.15	4.42	L→LV
308.15	2.80	L→LV	308.15	4.24	L→LV	308.15	5.77	L→LV
323.15	3.35	L→LV	323.15	5.16	L→LV	323.15	7.13	L→LV
338.15	3.89	L→LV	338.15	6.08	L→LV	338.15	8.48	L→LV
358.15	4.62	L→LV	358.15	7.30	L→LV	358.15	10.29	L→LV
378.15	5.35	L→LV	378.15	8.52	L→LV	378.15	12.10	L→LV
$z_{\text{CO}_2} = 50.18 \pm 0.07 \text{ mol } \%$			$z_{\text{CO}_2} = 60.18 \pm 0.03 \text{ mol } \%$			$z_{\text{CO}_2} = 70.17 \pm 0.03 \text{ mol } \%$		
293.15	5.30	L→LV	293.15	15.43	L→LL	293.15	50.90	L→LL
308.15	7.27	L→LV	308.15	12.52	L→LL	308.15	28.93	L→LL
323.15	9.25	L→LV	323.15	14.01	L→LV	323.15	24.62	L→LV
338.15	11.22	L→LV	338.15	16.15	L→LV	338.15	24.50	L→LV
358.15	13.85	L→LV	358.15	19.01	L→LV	358.15	26.08	L→LV
378.15	16.48	L→LV	378.15	21.86	L→LV	378.15	28.24	L→LV
$z_{\text{CO}_2} = 75.15 \pm 0.02 \text{ mol } \%$			$z_{\text{CO}_2} = 80.13 \pm 0.02 \text{ mol } \%$			$z_{\text{CO}_2} = 85.10 \pm 0.01 \text{ mol } \%$		
308.15	36.92	L→LL	308.15	50.48	L→LL	308.15	60.97	L→LL
323.15	29.75	L→LV	323.15	33.93	L→LL	323.15	37.37	L→LL
338.15	28.40	L→LV	338.15	31.04	L→LV	338.15	34.80	L→LV
358.15	29.14	L→LV	358.15	31.29	L→LV	358.15	33.14	L→LV
378.15	30.58	L→LV	378.15	32.52	L→LV	378.15	33.13	L→LV
$z_{\text{CO}_2} = 90.07 \pm 0.01 \text{ mol } \%$			$z_{\text{CO}_2} = 95.03 \pm 0.01 \text{ mol } \%$					
293.15			293.15	17.89	V→LV			
308.15	41.99	F→FF	308.15	18.67	V→LV			
323.15	33.69	F→FF	323.15	20.10	V→LV			
338.15	32.58	V→LV	338.15	22.36	V→LV			
358.15	31.14	V→LV	358.15	25.12	V→LV			
378.15	32.90	V→LV	378.15	27.90	V→LV			

633

634 Table 7. Critical temperature, critical pressure, and acentric factor for chemical compounds

compound	$P_c$ , MPa	$T_c$ , K	$\omega$
CO <sub>2</sub> <sup>a</sup>	7.380	304.20	0.225
diphenylmethane <sup>b</sup>	2.979	767.0	0.475

635 <sup>a</sup> from NIST webbook database [87]. <sup>b</sup>  $P_c$  and  $T_c$  from NIST webbook database [87] and  $\omega$

636 calculated from Eq. (4).

637

638

639

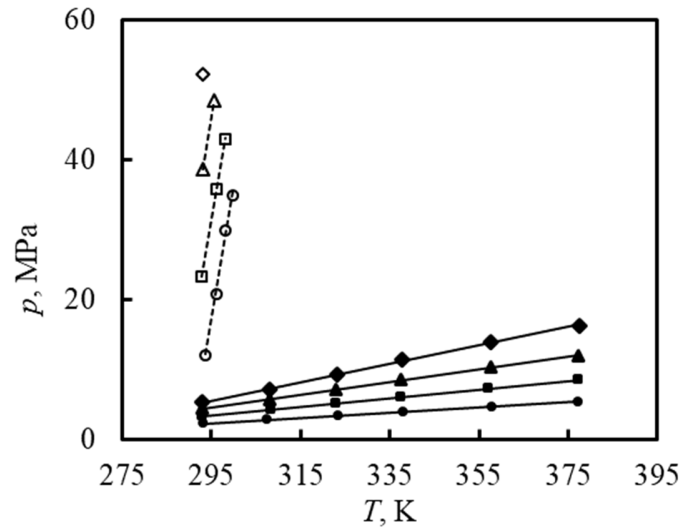
640

641 Table 8. Fitted and predicted binary interaction parameters obtained at different  
642 temperatures for PR and PPR78 models.

$T, K$	Fitted $k_{ij}$	PPR78 $k_{ij}$
293.15	0.0996	0.0973
308.15	0.0979	0.0949
323.15	0.0961	0.0934
338.15	0.0946	0.0927
358.15	0.0924	0.0925
378.15	0.0900	0.0930

643

644



645

646 Figure 1. Isophletic  $pT$  phase diagram for the  $\text{CO}_2$  – diphenylmethane mixtures with bubble  
 647 point pressures (L→LV, solid symbols) and liquid – solid phase transitions ( L→LS, unfilled

648 symbols) at several feed compositions. ●, ○:  $z_{\text{CO}_2} = 20.12$  mol %; ■, □:  $z_{\text{CO}_2} = 30.20$   
 649 mol %; ▲, △:  $z_{\text{CO}_2} = 40.20$  mol %; and: ◆, ◇:  $z_{\text{CO}_2} = 50.18$  mol %. Lines included for

650 eye-guide.

651

652

653

654

655

656

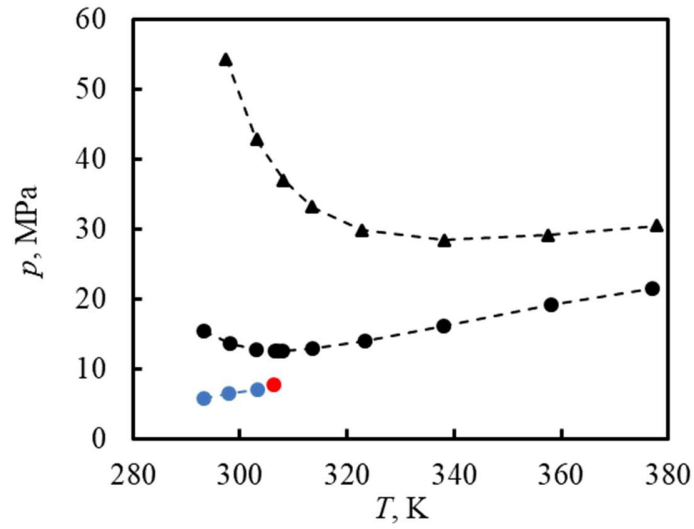
657

658

659

660

661



662

663 Figure 2. Isophletic  $pT$  phase diagram for the  $CO_2$  – diphenylmethane mixtures with phase  
 664 transitions at several feed compositions. Biphasic envelope ( $L \rightarrow LV$  and  $L \rightarrow LL$ ) for ●:  
 665  $z_{CO_2} = 60.18$  mol %; and ▲:  $z_{CO_2} = 75.15$  mol %. ●: Liquid – liquid – vapor equilibrium  
 666 ( $LL \rightarrow LLV$ ) for  $z_{CO_2} = 75.15$  mol %; and ●: LLV triphasic UCEP. Dashed lines included  
 667 for eye-guide.

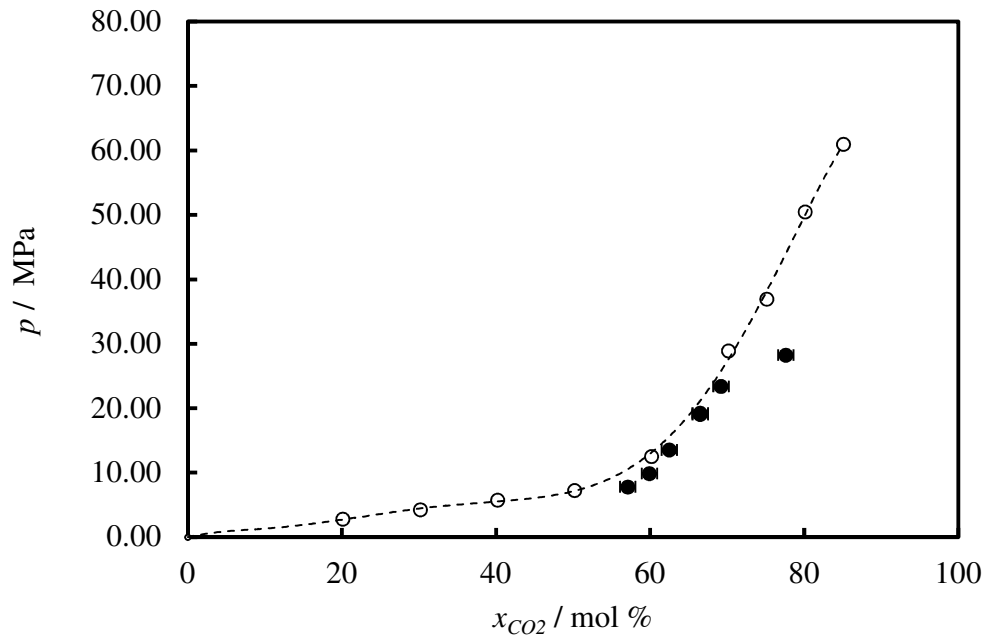
668

669

670

671

672



673

674 Figure 3. Comparison between liquid phase composition reported by Chung et al. [75] (●)

675 and the present work (○)for carbon dioxide and diphenylmethane binary system at 308.15

676 K.

677

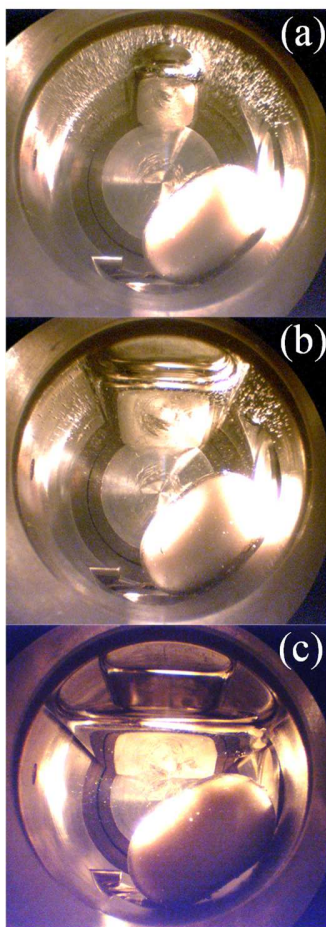
678

679

680

681





682

683 Figure 4. Observed phase equilibria during isothermal depressurization of CO<sub>2</sub> and  
684 diphenylmethane mixtures: (a) liquid – liquid equilibrium for  $z_{CO_2} = 60.18$  mol % at 293.2  
685 K and 10.0 MPa; (b) liquid – liquid – vapor equilibrium for  $z_{CO_2} = 60.18$  mol % at 293.2 K  
686 and 5.70 MPa; (c) liquid – liquid – vapor equilibrium for  $z_{CO_2} = 75.15$  mol % at 292.8 K  
687 and 5.57 MPa.

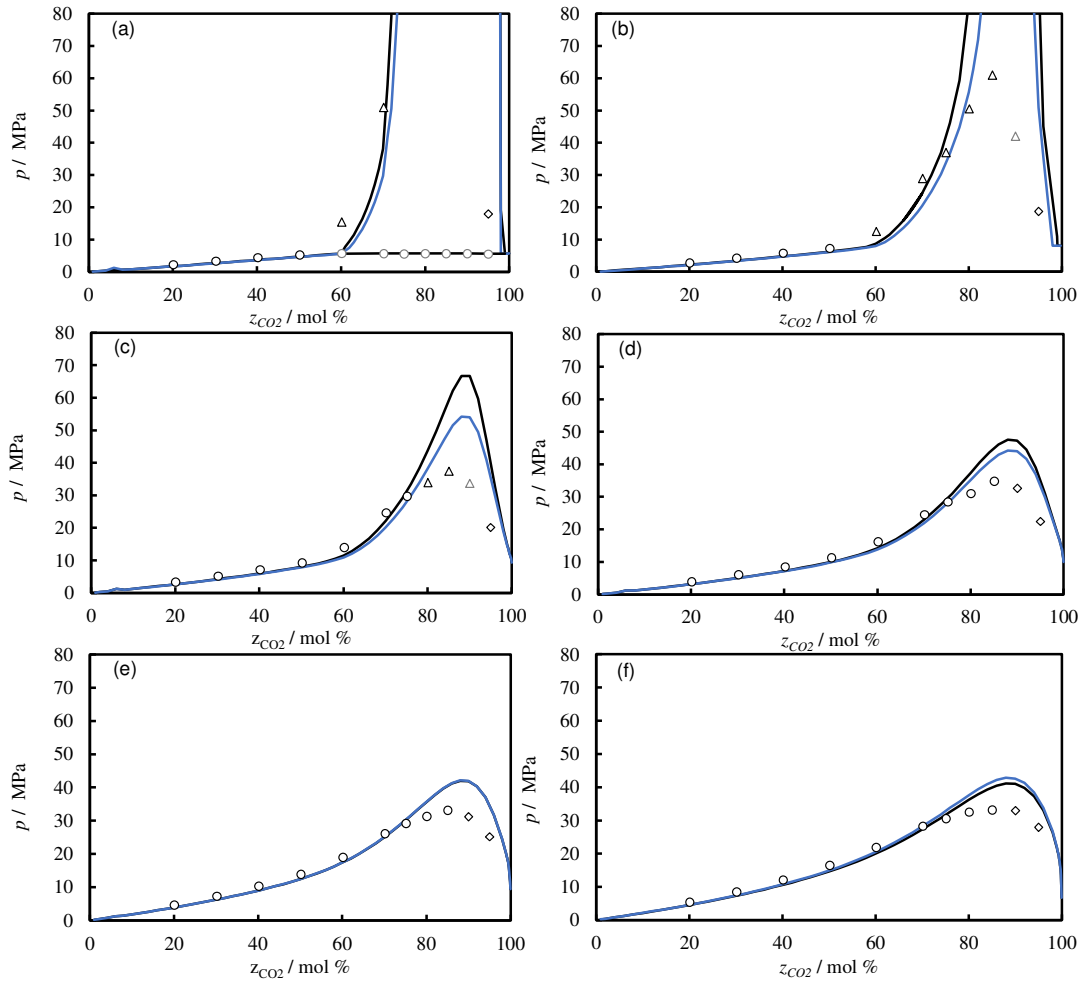
688

689

690

691

692



693

694 Figure 5. Isothermal interpolated  $p$ - $z_{CO_2}$  diagram at different temperatures  $T = 293.15$  K (a);  
 695  $T = 308.15$  K (b);  $T = 323.15$  K (c);  $T = 338.15$  K (d);  $T = 358.15$  K (e); and  $T = 378.15$  K (f)  
 696 compared to modelling results from PR EOS with fitted binary interaction parameters from  
 697 Table 7 (black line), and PPR78 model (blue line). Experimental L→LV in black circles  
 698 (○); L→LL in black triangles (△), F→FF in gray triangles (△); LL→LLV in gray circles  
 699 (○); and V→LV in diamonds (◇).

700

# Fluid phase equilibria in asymmetric model systems.

## Part I: CO<sub>2</sub> + diphenylmethane

J.F. Romero Yanes, J. P. Bazile, F. Montel, J.L. Daridon

Laboratoire des Fluides Complexes et leurs Réservoirs E2S UPPA, CNRS, TOTAL ENERGIES, LFCR,

Université de Pau et des Pays de l'Adour, Pau, 64000, France

### Graphical Abstract

